# Supporting Information for

# East Asian Anthropogenic Aerosols Strongly Influence Past and Present Southern African Hydroclimate and Ecosystem Changes

Bosi Sheng[1,2,*], Massimo A. Bollasina[2], Alexandre S. Gagnon[3], Laura J. Wilcox[4], Thomas P. S. Reynolds[1], Christopher T. S. Beckett[1], Haolin Wang[2], Qingxiang Li[5], Pierre Nabat[6], Robert J. Allen[7], Bjørn H. Samset[8], Joonas Merikanto[9], Geeta G. Persad[10], Toshihiko Takemura[11], Kostas Tsigaridis[12,13], Sharar Ahmadi[4], Maxwell T Elling[14,15], Knut von Salzen[16,17], Daniel M Westervelt[18], Naga Oshima[19], Tsuyoshi Koshiro[19]

[1] Institute for Infrastructure and Environment, School of Engineering, University of Edinburgh, UK

[2] School of GeoSciences, University of Edinburgh, UK

[3] School of Biological and Environmental Sciences, Liverpool John Moores University, UK

[4] National Centre for Atmospheric Science, Department of Meteorology, University of Reading, UK

[5] School of Atmospheric Sciences, Sun Yat-Sen University, and Key Laboratory of Tropical Atmosphere-Ocean System, Ministry of Education, China

[6] Météo-France, CNRS, Univ. Toulouse, CNRM, Toulouse, France

[7] Department of Earth and Planetary Sciences, University of California Riverside, Riverside, CA, USA

[8] CICERO Center for International Climate Research, Oslo, Norway

[9] Finnish Meteorological Institute, Climate Research, Helsinki, Finland

[10] Department of Geological Sciences, The University of Texas at Austin, Austin, TX, USA

[11] Research Institute for Applied Mechanics, Kyushu University, Fukuoka, Japan

[12] Center for Climate Systems Research, Columbia University, New York, NY, USA

[13] NASA Goddard Institute of Space Studies, New York, NY, USA

[14] Department of Atmospheric and Oceanic Sciences, University of Colorado Boulder, Boulder, CO, USA

[15] Cooperative Institute for Research in Environmental Sciences, University of Colorado Boulder, Boulder, CO, USA

[16] Canadian Centre for Climate Modelling and Analysis, Environment and Climate Change Canada, Victoria, BC, Canada

[17] Department of Atmospheric and Climate Science, University of Washington, Seattle, WA, USA

[18] Lamont-Doherty Earth Observatory, Columbia Climate School, New York, NY, USA

[19] Meteorological Research Institute, Japan Meteorological Agency, Ibaraki, Japan

Correspondence: Bosi Sheng (bsheng@ed.ac.uk)

**This PDF file includes:**

Supporting Table S1 to S3 and Figure S1 to S7

**Table S1.** CMIP6 models included in this study that performed the hist-All, hist-GHG, and hist-AER simulations, with corresponding ensemble sizes and horizontal resolution.

| Model name | Ensembles | Horizontal resolution |
|---|---|---|
| ACCESS-CM2 | 3 | 1.3° × 1.9° |
| ACCESS-ESM1-5 | 3 | 1.3° × 1.9° |
| CNRM-CM6-1 | 10 | 1.4° × 1.4° |
| E3SM-2-0 | 5 | 1.0° × 1.0° |
| FGOALS-g3 | 3 | 2.0° × 2.25° |
| HadGEM3-GC31-LL | 10 | 1.3° × 1.9° |
| IPSL-CM6A-LR | 10 | 1.3° × 2.5° |
| MIROC6 | 10 | 1.4° × 1.4° |
| MRI-ESM2-0 | 5 | 1.1° × 1.1° |
| NorESM2-LM | 3 | 1.9° × 2.5° |

**Table S2.** List of PDRMIP models from CMIP5 used in this study.

| Model name | Horizontal resolution | Aerosol setting |
|---|---|---|
| GISS-E2-R | 2.0° × 2.5° | Fixed concentrations |
| HadGEM3 | 1.3° × 1.9° | Fixed concentrations |
| IPSL-CM5A | 1.9° × 3.8° | Fixed concentrations |
| MIROC-SPRINTARS | 1.4° × 1.4° | HTAP2 Emissions |
| NCAR-CESM1-CAM4 | 1.9° × 2.5° | Fixed concentrations |
| NCAR-CESM1-CAM5 | 1.9° × 2.5° | Emissions |
| NorESM1-M | 1.9° × 2.5° | Fixed concentrations |

**Table S3.** List of RAMIP models used in this study.

| Model name | Ensembles | Horizontal resolution | Data source |
|---|---|---|---|
| CanESM5-1 | 10 | 2.8° × 2.8° | [1] |
| CESM2 | 10 | 1.0° × 1.3° | [2] |
| CNRM-ESM2-1 | 10 | 1.4° × 1.4° | [3] |
| EC-Earth3-AerChem | 10 | 0.7° × 0.7° | [4] |
| GISS-E2-1-G | 10 | 2.0° × 2.5° | [5] |
| MIROC6 | 10 | 1.4° × 1.4° | [6] |
| MRI-ESM2-0 | 10 | 1.1° × 1.1° | [7] |
| NorESM2-LM | 10 | 2.0° × 2.5° | [8] |
| SPEAR | 10 | 1.0° × 1.3° | [9] |
| UKESM1-0-LL | 10 | 1.3° × 1.9° | [10] |


[1] Fraser-Leach, L.; Kushner, P.; von Salzen, K.; Swart, N. (2025): CanESM5-1 output prepared for the Regional Aerosol Model Intercomparison Project (RAMIP). NERC EDS Centre for Environmental Data Analysis, date of citation. http://catalogue.ceda.ac.uk/uuid/a33a7cc2d0a84e27a78b24d70fe257e4

[2] Allen, R. (2026): CESM2 output prepared for the Regional Aerosol Model Intercomparison Project (RAMIP). NERC EDS Centre for Environmental Data Analysis, *date of citation*. http://catalogue.ceda.ac.uk/uuid/b7c87e4dafcc486ba1eca2abac752abf

[3] Nabat, P. (9999): CNRM-ESM2-1 output prepared for the Regional Aerosol Model Intercomparison Project (RAMIP). NERC EDS Centre for Environmental Data Analysis, date of citation. http://catalogue.ceda.ac.uk/uuid/5477e60b209a4e169ca60d7f01a017eb

[4] O'Donnell, D.; Makkonen, R.; Merikanto, J. (2025): EC-Earth3-AerChem output prepared for the Regional Aerosol Model Intercomparison Project (RAMIP). NERC EDS Centre for Environmental Data Analysis, *date of citation*. http://catalogue.ceda.ac.uk/uuid/d581329422fb455ab9af0ea96c04d266

[5] Data to be released.

[6] Takemura, T. (9999): MIROC6 output prepared for the Regional Aerosol Model Intercomparison Project (RAMIP). NERC EDS Centre for Environmental Data Analysis, date of citation. http://catalogue.ceda.ac.uk/uuid/7fbe5be720a34d4785cc7e3bb9df4641

[7] Oshima, N.; Koshiro, T. (2025): MRI-ESM2-0 output prepared for the Regional Aerosol Model Intercomparison Project (RAMIP). NERC EDS Centre for Environmental Data Analysis, date of citation. http://catalogue.ceda.ac.uk/uuid/e8678aaf39144d8cb10cd02e8a562101

[8] Lewinschal, A. (2025): NorESM2-LM output prepared for the Regional Aerosol Model Intercomparison Project (RAMIP). NERC EDS Centre for Environmental Data Analysis, *date of citation*. http://catalogue.ceda.ac.uk/uuid/44100d99d120487284d7b778dbc76bdf

[9] Data to be released.

[10] Rumbold, S.; Keeble, J.; Wilcox, L.; Ahmadi, S.; Griffiths, P.; Lister, G.; Predoi, V. (2026): UKESM1-0-LL output prepared for the Regional Aerosol Model Intercomparison Project (RAMIP). NERC EDS Centre for Environmental Data Analysis, date of citation. http://catalogue.ceda.ac.uk/uuid/63233813672245a2ba3c6de90c4cfaee

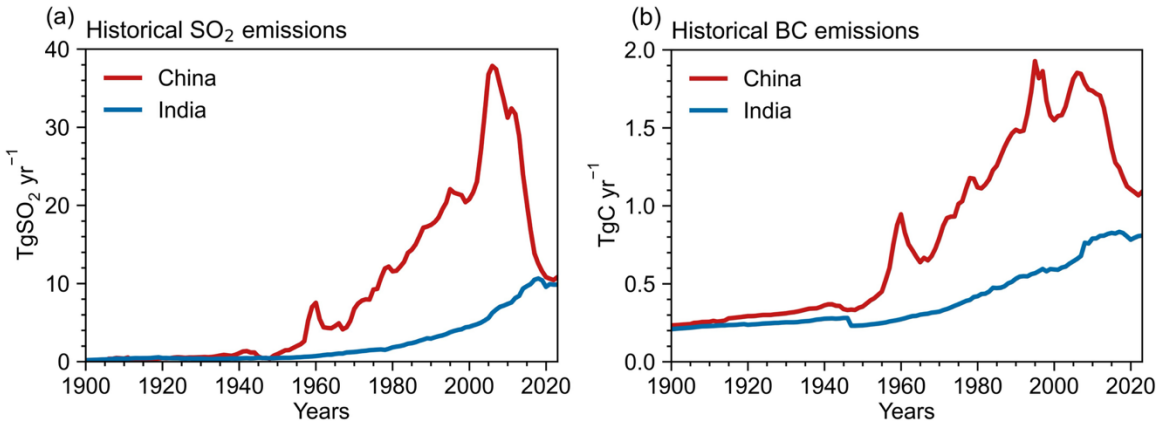


**Figure S1.** Trends in annual anthropogenic emissions of (**a**) sulfur dioxide ($SO_2$) and (**b**) black carbon (BC) over China and India over 1900–2023, based on the CEDS inventory. $SO_2$ emissions over China peak in the mid-2000s (around 2005–2007) before declining sharply.

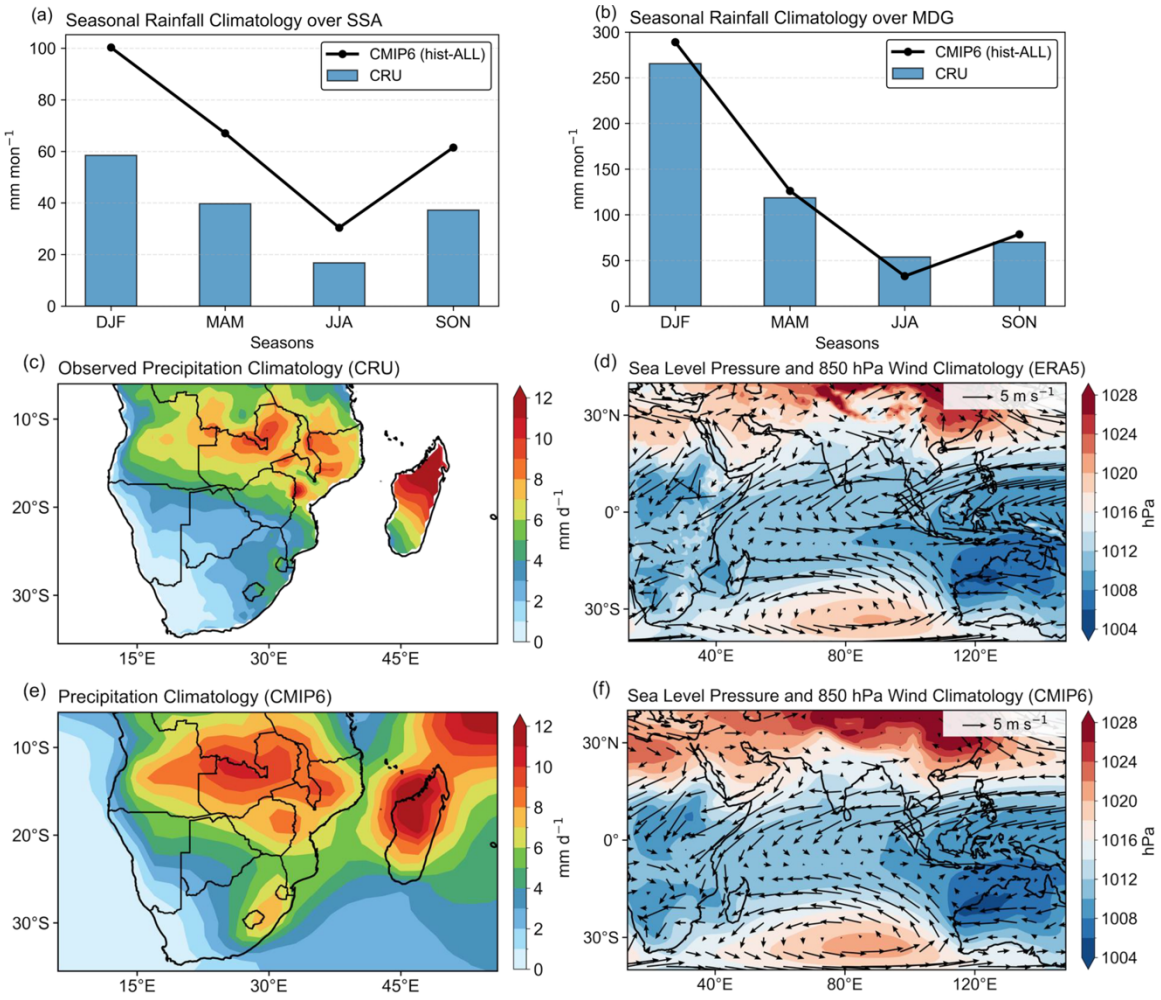


**Figure S2.** The DJF precipitation climatology (1961–1990) over (a) SSA and (b) MDG from CMIP6 hist-All simulations and CRU observations. Spatial distribution of the DJF climatological mean (1961–1990): (c) precipitation (CRU); (d) mean sea level pressure (shading) and 850 hPa winds (vectors) (ERA5); (e) precipitation (CMIP6 hist-All MMM); (f) mean sea level pressure (shading) and 850 hPa winds (vectors) (CMIP6 hist-All MMM).

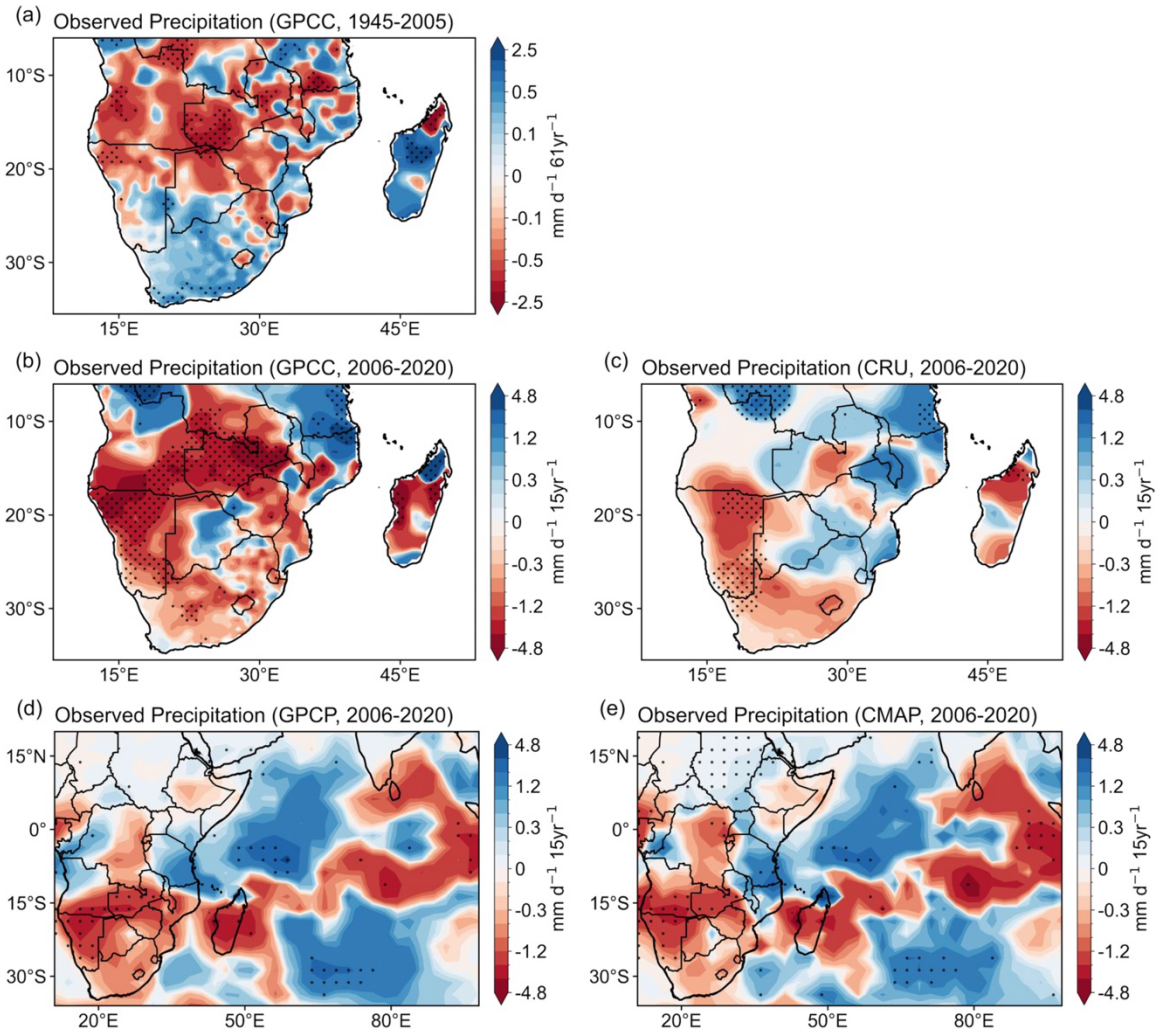


**Figure S3.** Spatial distribution of linear trends in DJF precipitation derived from (**a**) GPCC for 1945–2005, (**b**) GPCC for 2006–2020, (c) CRU for 2006–2020, (**d**) GPCP for 2006–2020, and (**e**) CMAP for 2006–2020.

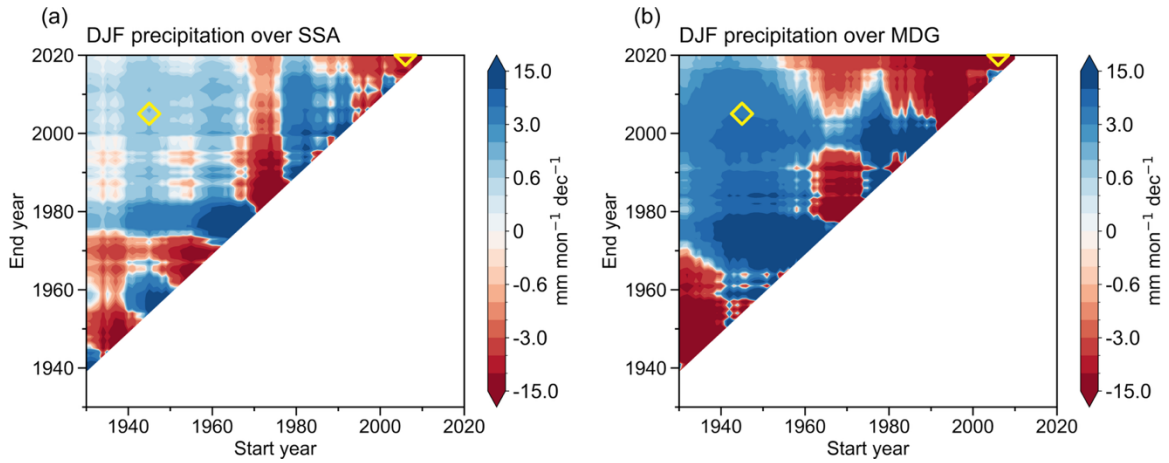


**Figure S4.** Observed DJF precipitation trends over (**a**) SSA and (**b**) MDG as a function of start and end years during the twentieth century, based on CRU observational data. All trends with a minimum length of 10 years are shown. Yellow diamonds indicate the two analysis periods used in this study (1945–2005 and 2006–2020). The consistent sign of trends across a wide range of start–end year combinations indicates that the identified changes are robust.

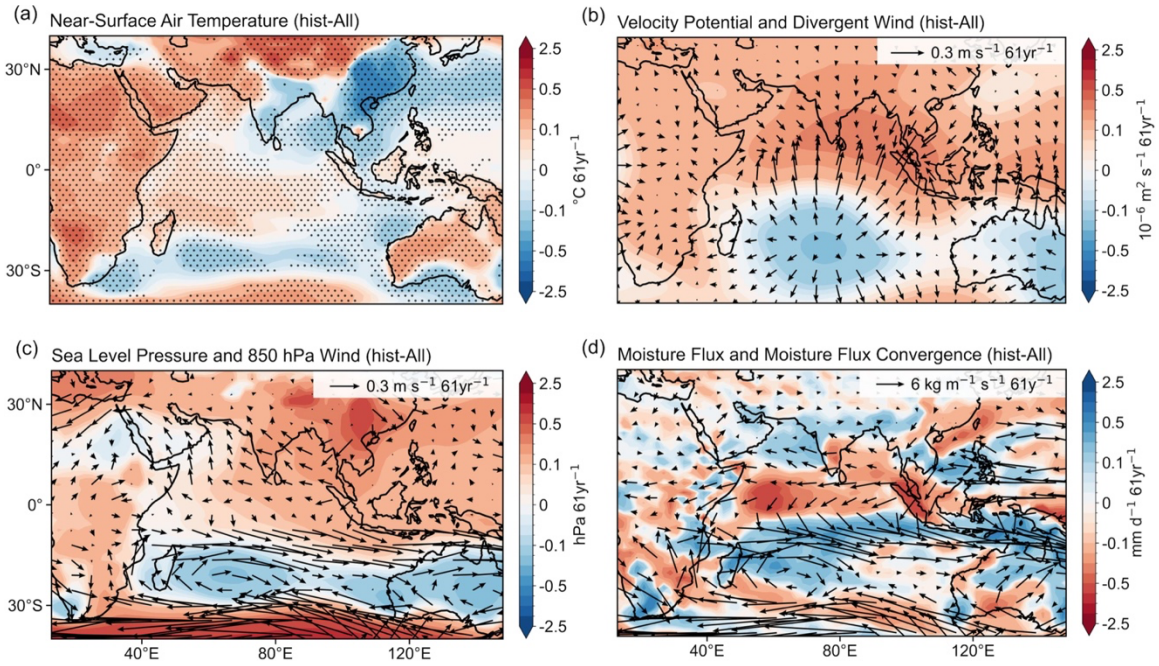


**Figure S5.** Spatial distribution of DJF trends over 1945–2005: (a) near-surface temperature relative to the contemporaneous tropical ocean mean (25°S–25°N), (b) velocity potential (shading) with divergent wind (vectors) at 200 hPa, (c) mean sea level pressure (shading) with 850 hPa winds (vectors), and (d) vertically integrated moisture flux (vectors) and moisture flux convergence (shading) for the hist-All simulations. All trends are based on the multimodel mean (MMM) across 10 CMIP6 models. Stippling indicates regions where at least 70% of models agree on the sign of change.

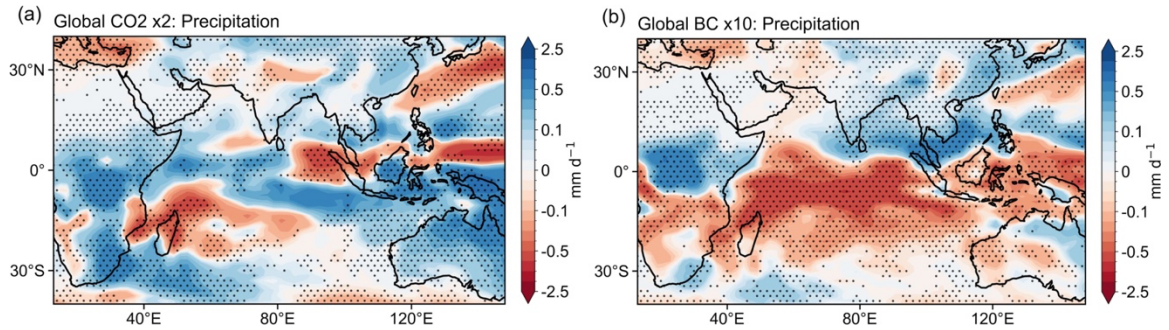


**Figure S6.** Spatial anomalies of DJF precipitation from PDRMIP experiments. Panels (**a**) and (**b**) show the total equilibrium precipitation response in the Global $CO_2$×2 and Global BC×10 simulations, respectively. Seven models were used to calculate the multimodel mean, and stippling indicates regions where at least 70% of the models agree on the sign of change.

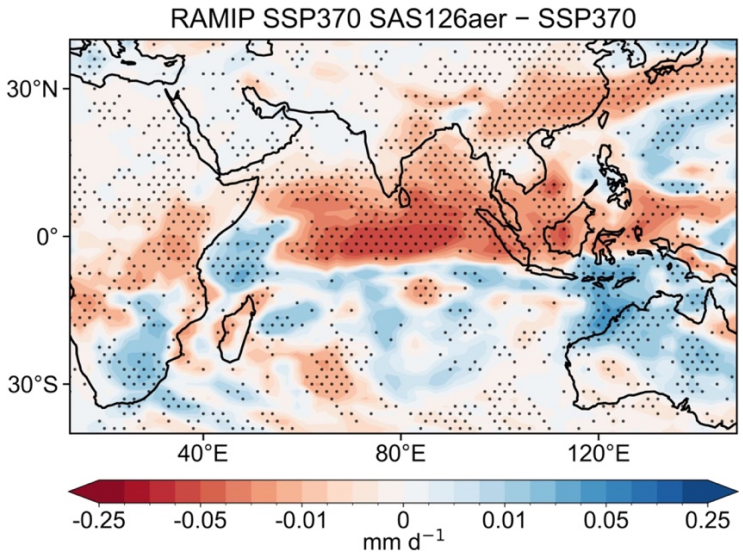


**Figure S7.** Spatial distribution of DJF mean precipitation changes over 2035–2049 from RAMIP simulations, shown as the MMM across 10 models (100 ensemble members). Results are defined as the difference between the South Asian perturbation (SSP370-SAS126aer) and the baseline simulation (SSP370). As aerosol emissions over SAS have shown only a modest increase in recent decades—substantially smaller than the perturbation applied in RAMIP—the simulated response is rescaled (sign –of 5) to better approximate observed changes. Stippling indicates regions where at least 70% of models agree on the sign of change.